Application of a first-principles anomalous transport model for electrons to multiple Hall thrusters and operating conditions

Alejandro Lopez Ortega,[1] Ira Katz[2] and Vernon H. Chaplin[3]
Jet Propulsion Laboratory, California Institute of Technology, Pasadena, CA, 91109, USA

Abstract: We have developed a physics-based model based on a pseudo-particle description of the electron cyclotron drift instability. A key improvement of the model with respect to previous work is that linear theory is not applied in the event of wave saturation and deviations of electrons or ions from a Maxwellian distribution function. In the acceleration region, the anomalous collision frequency is computed as the minimum value necessary to prevent the electron drift velocity from exceeding the thermal velocity. A functional based on the electron equilibration time is defined to control the transition from high to low resistivity regions. The model was previously applied to a single Hall thruster at its nominal operating condition, showing promising results that captured accurately the location of the thruster's acceleration region. In this paper, we extend the use of this first-principles models to two additional thrusters, also considering multiple operating conditions for each of them. Numerical results are compared to experimental measurements obtained with non-invasive laser induced fluorescence. In general, the agreement between experiments and simulations is good. The model is able to predict the location of the acceleration region for all cases. We observe however that fine details, such as changes in the plasma potential gradient within the acceleration regions, are not captured. The model is also insensitive to changes in the magnetic field strength while experiments show that small shifts in location (of less than 5% of the acceleration channel length) occur. We plan to address the weaknesses of our method with the help of physical insight gained from kinetic simulations of the acceleration region.

I. Nomenclature

$\mathbf{B}$	=	magnetic field
B	=	magnitude of magnetic field
c_s	=	ion sound speed
$\mathbf{E}$	=	electric field
e	=	elementary charge
ε_0	=	vacuum permittivity
F_a	=	anomalous force
$\mathbf{j}_s$	=	current density of species s
k	=	wavenumber modulus
λ_{De}	=	electron Debye length
L	=	length of thruster channel
m	=	mass
n	=	number density

[1] Member of the Technical Staff, Electric Propulsion Group, 4800 Oak Grove Drive, Pasadena, CA, 91109, Mail Stop 125-109, Member AIAA
[2] Principal Engineer, Electric Propulsion Group, 4800 Oak Grove Drive, Pasadena, CA, 91109, Mail Stop 125-109, Associate Fellow AIAA.
[3] Member of the Technical Staff, Electric Propulsion Group, 4800 Oak Grove Drive, Pasadena, CA, 91109, Mail Stop 125-109, Member AIAA

N_k = wave action for wavenumber k
$N_{k,sat}$ = wave action at saturation for wavenumber k
Ω_e = Hall parameter
T = temperature (in eV)
τ = isotropization time
$\mathbf{u}$ = velocity vector
v_s = thermal velocity of species s
ν_a = anomalous collision frequency
ν_{ei} = electron-ion collision frequency
ν_{en} = electron-neutral collision frequency
ν_{in} = ion-neutral collision frequency
$\omega_{i,k}$ = imaginary part of the wave frequency
$\omega_{i,klinear}$ = imaginary part of the wave frequency in linear theory
ω_{ie} = linear electron contribution to the imaginary part of the wave frequency
ω_{ii} = ion contribution to the imaginary part of the wave frequency
e = (subscript) electron
i = (subscript) ion
n = (subscript) neutrals
$\perp$ = (subscript) direction perpendicular to magnetic field

II. Introduction

There exist two common approaches for conducting numerical simulations of Hall thrusters. Hydrodynamics formulations assume that the particles in the plasma conform to a Maxwellian distribution function and subsequently employ the zeroth, first and second moments of Boltzmann's equation with respect to the velocity field to solve for the spatial distribution of the bulk density, velocity and energy of the species in the plasma. Kinetic approaches on the other hand attempt to directly solve Boltzmann's equation as a function of space and velocity or, instead, make use of macro-particles that represent the different species in the plasma and move in the computational grid according to the Lorentz force. While kinetic formulations can be applied in three dimensions to ions and neutrals in Hall thruster plasmas, 3-D kinetic simulations of electrons are not possible to date, due to the small lengths and time-scales associated with the Debye length and electron plasma frequency. The latter restricts kinetic simulations of electrons to 1-D or 2-D configurations, in which at least one direction is omitted. These simulations may not be representative of a realistic Hall thruster geometry. For engineering applications, hydrodynamics formulations have been favored as they enable computations in realistic geometries at moderate computational cost. Hydrodynamics simulations can then be employed for purposes such as predicting performance and erosion of the walls, and guiding the design of Hall thrusters.

The major impediment of hydrodynamics codes is that an algorithm dependent only on physical first-principles has not been possible to date. The reason for this is that classical collision theory predicts resistivity values across magnetic field lines much larger than those required for reproducing the experimentally observed plasma measurements. Historically, numerical and analytical studies have accounted for this phenomenon by introducing an anomalous collision frequency term in the computation of transport coefficients. This anomalous collision frequency effectively reduces the Hall parameter and therefore the resistivity. Results obtained using codes such as Hall2De [1-2] improve when the anomalous collision frequency term is informed by experimental measurements. Kinetic simulations that self-consistently model the electron drift in the azimuthal and either the radial [3] or the axial directions [4-5] have exhibited lower overall resistivity values than those predicted by classical collisions, qualitatively capturing the phenomenon that is modeled as anomalous collision frequency in hydrodynamics codes. However, the simplified geometry considered in these simulations makes this approach inapplicable for engineering purposes.

The physical process or processes that facilitate the transport of electrons across magnetic field lines in a Hall thruster are not fully understood. One leading theory, initially proposed by Adam et al. [4], is that the turbulence generated by the electron cyclotron drift instability (ECDI) [6] is the cause of the anomalous electron transport in a Hall thruster. The ECDI is similar to the ion-acoustic instability (IAI) [7-10] in the sense that large electron drift velocities amplify the instability and that the wave frequency is proportional to the ion sound speed. In Hall thrusters, the ExB drift in the azimuthal direction is the suspected source of the instability. The presence of ECDI in Hall thrusters has been confirmed experimentally [11-12], by analysis [12-13], and by means of one-dimensional [14] and two-dimensional [4-5] PIC simulations. The latter have shown enhanced electron transport as the ECDI develops and

transitions into the ion acoustic instability at large wave magnitudes [15]. One key aspect that merits further research is the fact that kinetic simulations and theory predict that waves grow in the acceleration region, a region of the Hall thruster defined by a steep gradient in the plasma potential that accelerates the ions. Since linear instability theory predicts that the wave magnitude is directly proportional to the anomalous collision frequency, one may expect the resistivity to be low in the acceleration region. However, our hydrodynamics simulations suggest that in order to achieve a steep plasma potential gradient, the anomalous collision frequency must be minimum and the resistivity maximum. In a companion paper [16], we discuss the results of two-dimensional kinetic simulations conducted in our group. These simulations focus on the acceleration region and the region immediately downstream in the direction of ion motion (typically referred to as the plume) and suggest that the waves generated in the acceleration region are convected by the ions. The electrons in the plume, which move in the opposite direction to the ions, interact with the waves and behave as unmagnetized electrons. However, as the electron distribution increases in temperature moving from the plume into the acceleration region, the electrons become magnetized and the interaction with the waves is minimized, with waves minimally contributing to electron transport across magnetic field lines in the acceleration region. A steep plasma potential gradient is then required to transport electrons across the acceleration region. We also observe that the electrons in the acceleration region exhibit significant deviations from the Maxwellian distribution function that is assumed in hydrodynamics codes.

In [17], we presented a physics-based model, based on a pseudo-particle description of ECDI waves, that enabled the computation of the anomalous collision frequency as implemented in our hydrodynamics code Hall2De [1-2]. The key improvement of this model with respect to previous work was decoupling the linear theory correlation that exists between the anomalous collision frequency and the magnitude of the wave perturbations in the event of wave saturation and deviation from a Maxwellian distribution function. We made use of plasma properties to compute the probability of electrons and/or ions having non-Maxwellian distribution functions. We then employed this model to produce numerically stable, first-principles simulations of the H6 unshielded (H6US) thruster [18] at 300 V, 20 A. Compared to that inferred by experiments, the computed location of the acceleration region was found to be within 10% of the channel length. The simulations also captured well the plasma gradients along the channel centerline of this thruster.

In this article, we use the model presented in [17] to conduct hydrodynamics simulations of other thrusters, such as the magnetically shielded H6 (H6MS) [19-20] and HERMeS [21-22] for a wide range of operating conditions. Numerical results are subsequently compared to experimental measurements, provided by laser-induced fluorescence (LIF) [23-24]. LIF is a non-intrusive experimental technique that enables the reconstruction of the ion velocity distribution function at multiple locations in the thruster. Reconstruction of the average velocity can be used in turn to determine the location of the acceleration region and the plasma potential field. This article is organized as follows. In Section III, we summarize the first-principles anomalous collision frequency model, as presented in [17]. In Section IV and V, we present and discuss the results of our simulations of the H6MS and HERMeS, respectively. Section VI outlines the main conclusions of this work and proposes directions for future research efforts.

III. Summary of first-principles model for anomalous transport in Hall thrusters

This section summarizes the main equations that account for the presence of anomalous transport in Hall2De. For further information, we encourage the reader to refer to Section III in [17].

The magnitude of the waves in the plasma for a particular wavelength is tracked by the wave action, N_k. Making use of the assumption that the waves fundamentally develop in the azimuthal direction, we can write independent evolution equations for each wave length

$$\frac{\partial N_k}{\partial t} + \mathbf{u}_i \cdot \nabla N_k = 2\omega_{i,k} N_k, \tag{1}$$

where $\mathbf{u}_i$ is the average ion velocity and $\omega_{i,k}$ is the growth rate of the instability. In the case of linear waves, the growth rate can be determined from the solution of the dispersion relation for ion acoustic waves. However, we assume in our model that there exists a non-linear mechanism that produces saturation (i.e., cancellation of wave growth) at a certain value of the wave action. The simplest expression that captures this phenomenon can be written as

$$\omega_{i,k} = \omega_{i,k,linear}\left(1 - \frac{N_k}{N_{k,sat}}\right), \tag{2}$$

where $\omega_{i,k,linear}$ is the growth rate from linear theory

$$\omega_{i,k,linear} = \omega_{ie,linear} + \omega_{ii,linear}, \tag{3}$$

$$\omega_{ie,linear} = \frac{\sqrt{\pi} c_s k}{2\left(1+k^2\lambda_{De}^2\right)}\left(\frac{k u_e}{\nu_e k} - \frac{c_s}{\nu_e\left(1+k^2\lambda_{De}^2\right)^{1/2}}\right), \tag{4}$$

$$\omega_{ii,linear}=-\frac{\sqrt{\pi}c_s k}{2\left(1+k^2\lambda_{De}^2\right)^{3/2}}\frac{T_e}{T_i}\left(\frac{c_s}{v_i\left(1+k^2\lambda_{De}^2\right)^{1/2}}\right)\exp\left(-\left(\frac{c_s}{v_i\left(1+k^2\lambda_{De}^2\right)^{1/2}}\right)^2\right)-\frac{\nu_{in}}{2}, \quad (5)$$

with T_e and T_i the electron and ion temperature, respectively, u_e the electron velocity in the azimuthal direction, $v_s=\sqrt{2eT_s/m_s}$ the thermal velocity, $c_s=\sqrt{2eT_e/m_i}$ the sound speed, and $\lambda_{De}=\sqrt{\varepsilon_0 T_e/(en_0)}$ the Debye length. $N_{k,sat}$ is the value of the wave action that produces saturation of the instability. PIC simulations [16] have shown that the oscillations in plasma potential are relatively small and do not exceed T_e. Since the wave action is related to the amplitude of the oscillations, we can relate the electron temperature with the value of the wave action at saturation:

$$N_{k,sat}=\frac{n_0 T_e}{4c_s k\left(1+k^2\lambda_{De}^2\right)^{1/2}}. \quad (6)$$

In order to bring closure to the hydrodynamics equations in Hall2De, we need to relate the wave action to zeroth-order effects in the background plasma solution. Taking the first moment of Boltzmann's equation for electrons in the presence of a magnetic field, classical collisions, and wave perturbations, we obtain

$$0=-n_0 e\mathbf{E}-n_0 e u_e\times\mathbf{B}-\nabla(n_0 eT_e)-n_0 m_e(\nu_{ei}(\mathbf{u}_e-\mathbf{u}_i)+\nu_{en}\mathbf{u}_e)+\mathbf{F}_{a(e)}. \quad (7)$$

We also neglected the inertia terms and assumed that the neutral velocity is negligible (i.e., $\mathbf{u}_e>>\mathbf{u}_n$). $\mathbf{F}_{a(e)}$ represents the anomalous force due to wave perturbations which can be written as

$$\mathbf{F}_{a(e)}=-m_e n_0 \nu_a(\mathbf{u}_e-\mathbf{u}_i). \quad (8)$$

It was shown in [17] that the anomalous collision frequency can be related to the wave action and growth rate of the instability by

$$\nu_a=\frac{2e}{Nm_e n_0|\mathbf{u}_e-\mathbf{u}_i|}\sum_k kN_k\omega_{ie}, \quad (9)$$

where N is the number of discrete wavelengths considered in the simulation and ω_{ie} is the contribution of the electrons to the growth rate, which is only equal to (4) in case of Maxwellian electrons and $N_k<N_{k,sat}$. If ions are Maxwellian, we can compute a generalized expression for ω_{ie} as $\omega_{ik,sat}-\omega_{ii,linear}$. Thus, the anomalous collision frequency can be rewritten as

$$\nu_a=\frac{2e}{Nm_e n_0|\mathbf{u}_e-\mathbf{u}_i|}\sum_k kN_k\left\{(1-f)\omega_{ie,linear}+f\left(\omega_{i,k,sat}-\omega_{ii,linear}\right)\right\}. \quad (10)$$

The parameter *f* is determined from the background plasma parameters. We identify regions of the thruster in which the ions remain Maxwellian by comparing the equilibration time of ions, τ_{ii}, with the characteristic length of the thruster channel *L* and the ion velocity in the non-dimensional number,

$$K_i=\frac{L}{\tau_{ii}|u_i|}. \quad (11)$$

When $K_i>>1$ the ions are Maxwellian and we use the generalized expression for ω_{ie}, which in turn means that $f\sim1$. In order to determine whether electrons constitute a Maxwellian distribution, we compare the isotropization time for electrons with the velocity of the electrons perpendicular to the magnetic field and the characteristic length of the thruster,

$$K_e=\frac{L}{\tau_{ee}|u_e|}. \quad (12)$$

We now can define *f* as

$$f=\left(1-\exp(-K_e)\right)+\exp(-K_e)\exp(-K_i). \quad (13)$$

Note that when neither distribution is Maxwellian, $f\sim1$. The latter only occurs in the acceleration region (Fig. 1). However, we find in our simulations that $N_k=N_{k,sat}$ in the acceleration region (i.e., $\omega_{i,k,sat}=0$) and that the ion contribution $\omega_{ii,linear}$ is very small. Thus, in the acceleration region $\nu_a\sim0$. Recognizing that our model cannot be directly applied in the acceleration region, we make use of a criterion that prevents the electrons from exceeding the thermal speed instead:

$$\sqrt{\frac{2eT_e}{m_e}}\geq u_e\approx\Omega_e\frac{j_{e\perp}}{en_0}=\frac{eB}{m_e(\nu_{ei}+\nu_{en}+\nu_a)}\frac{j_{e\perp}}{en_0}, \quad (14)$$

where $j_{e\perp}$ is the electron current density perpendicular to the magnetic field lines and Ω_e is the Hall parameter. The floor value for the anomalous collision frequency then becomes

$$\nu_{a,floor}=\frac{B}{m_e n_0}\frac{j_{e\perp}}{\sqrt{\frac{2eT_e}{m_e}}}-\nu_{ei}-\nu_{en}, \quad (15)$$

The floor anomalous collision frequency can be interpreted as a simplified variable that accounts for the existence of other kinetic instabilities that prevent the electron drift from exceeding the electron thermal speed. These effects cannot be modeled based on the simplified theory of the ECDI presented here and may indeed involve other mechanisms that exhibit smaller time-scales, such as the two-stream instability of electrons and the Buneman instability. We plan on

using the lessons learned from the PIC simulations described in our companion paper [16] to improve our model of the acceleration region in the near future.

Numerical simulations use solutions with an experimentally informed anomalous collision frequency as initial conditions. During the transitory that occurs after the first-principles model is turned on, we impose f=0 in Eq. (10) for locations downstream of the peak magnetic field to avoid large fluctuations in the plasma that prevent the solution from reaching steady state. This constraint is consistent with the results of 2-D PIC simulations shown in [16], which predict Maxwellian electrons downstream of the peak magnetic field. After the solution with the first-principles model reaches steady state, we remove this condition. We also include a multiplying factor for the floor anomalous collision frequency (15). The value of this coefficient is determined so the simulations exactly match the operating condition in discharge voltage and current. We find in all the simulations shown in this article that the factor needed to exactly replicate the operating conditions is between 1 and 2. We consider the fact that the multiplying factor is order unity remarkable given that the floor anomalous collision frequency is actually a very simplified representation of the physics that occur in the acceleration region, where electrons and ions do not obey Maxwellian distribution functions. As we did in [17], we only consider singly charged ions in these simulations.

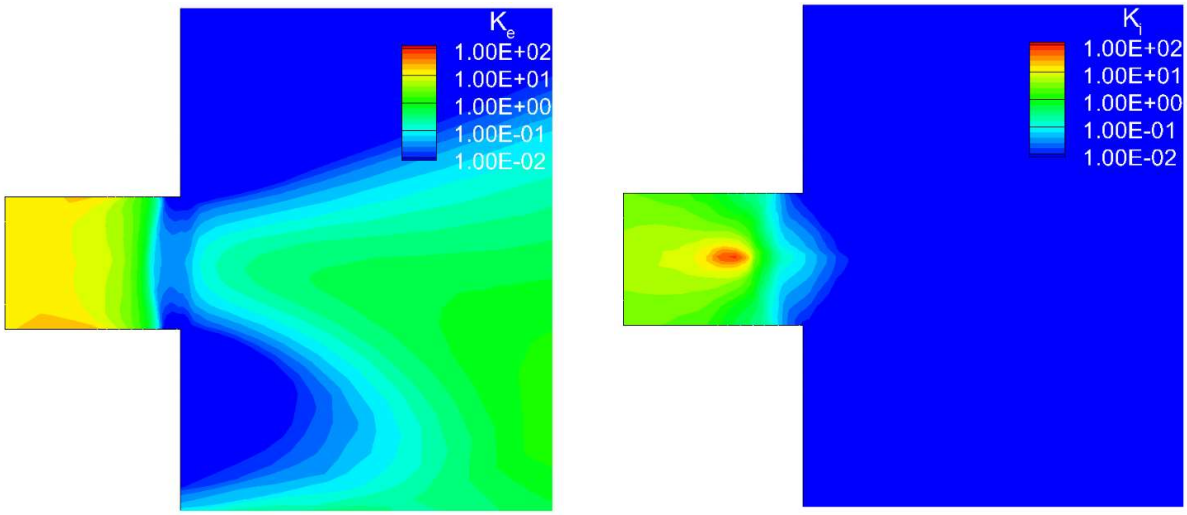

Figure 1. 2-D contour plot of K_e (12) and K_i (11) (non-dimensional thermal equilibration values for electron and ions, respectively) in the H6US at 300 V and 20 A.

IV. First-principles hydrodynamics simulations of the H6MS

The H6MS is a 6 kW-class Hall thruster that was developed as part of a proof-of-concept investigation of the magnetic shielding principles [19-20, 25]. This investigation involved a modification of the H6 laboratory Hall thruster from its original configuration, termed H6US and whose geometry was used in the simulations described in [9], to a magnetically shielded one with the guidance of modeling and simulation. In the first part of this section, we compare the results obtained by applying the method described in Section III to the H6US and H6MS at the nominal operating condition (300 V – 20 A). In the second part of this section, we explore the results produced by our model for multiple operating conditions of the H6MS and compare them to measurements obtained by LIF [23].

A. Comparison between results for the H6MS and H6US at 300 V – 20 A

As a result of magnetic shielding, the peak magnetic field along the channel centerline moves downstream. The acceleration region also moves downstream, as shown by LIF measurements of the ion velocity distribution function [23, 24]. In [17], we showed that the first-principles model for the anomalous collision frequency was able to capture the location of the acceleration region in the H6US with an error of less than 10% of the channel length. In [9], we showed two simulation scenarios that considered warm and cold ions. For simplicity, in this article we use the cold ion assumption in all our simulations.

Figure 2 depicts, for the H6MS and H6US, a comparison of the wave action for the first ten discrete wavenumbers between 500 m^{-1} and 5000 m^{-1}. With the assumption of cold ions, wave saturation occurs at the stagnation point of the velocity. Following Eq. (1), at the stagnation point the advection term is zero and the wave action always grows if the

right-hand side term is positive. The wave action is then advected from the stagnation point to the left and right. Since there is no effective damping (with the exception of the ν_{in} term in Eq.(5)), the wave action remains saturated in the entire computational domain, both for the H6MS and H6US. We showed in [17] that the main effect of considering warm ions was that the saturation of the wave action did not reach the region closest to the anode. The wave action in the acceleration region remained largely similar for cold and warm ions. Figure 3 shows the contribution to the anomalous collision frequency (Eq.(10)) of each of the discrete wavenumbers. We also include in this figure the floor anomalous collision frequency, computed using Eq. (15) and the total anomalous collision frequency. We have scaled the individual contributions of each wave number by N (number of discrete wave numbers) so they do not overlap with the total anomalous collision frequency. In both the H6US and H6MS, the value of the anomalous collision frequency computed by (10) is lower than the floor anomalous collision frequency starting at approximately z/L>0.7. This is because when f=1, and $N_k=N_{k,sat}$, $(1\text{-}f)\omega_{ie,linear}+f(\omega_{i,k,sat}\text{-}\omega_{ii,linear})\sim\nu_{in}/2$, which decreases as the neutrals get depleted in the ionization region. However, in the H6US, the conditions for f=0 (i.e., Maxwellian electrons) are met at approximately z/L=1 due to the upstream position of the peak magnetic field along the centerline. The latter translates into an increase in the anomalous collision frequency and decreased resistivity in the plume, as explained in more detail in [17]. On the other hand, the conditions for f=0 in the H6MS are met further downstream, at approximately z/L=1.7, a position commensurate with the more downstream location of the peak magnetic field. We also observe that the magnitude of the floor anomalous collision frequency is lower in the H6US than in the H6MS. Equation (15) states that the floor anomalous collision frequency is proportional to the magnetic field and the electron current density perpendicular to the field and inversely proportional to the density and the square root of the temperature. The profile of the magnetic field along the channel centerline is very similar for both thrusters, but the profile for the H6MS is shifted downstream by 0.13L. Note that this shift is different from the shift observed in the transition from f=1 to f=0 between H6MS and H6US, which suggests that the transition from a Maxwellian to a non-Maxwellian distribution function for electrons is not only dependent on the magnetic field but also on how the plasma properties respond to the new topology. From Fig. 5, we observe that the peak electron temperature has instead shifted between thrusters by 0.5L and the plasma density by approximately 0.4L. As a result, for locations that have the same magnetic field in both thrusters, the temperature in the H6MS is lower and the density slightly higher. As both thrusters share dimensions and operating condition, the electron current density must be very similar. Even though the lower temperature and higher density affect the floor anomalous collision frequency in opposite directions, the net result is a higher floor for the H6MS. In Fig. 4, the anomalous collision frequency for both thrusters is compared to classical collisions in the plasma. For the H6MS, due to the higher floor value, the anomalous collision frequency is dominant everywhere, while in the H6US there exists a region at z/L=0.6 for which the anomalous collision frequency becomes comparable to classical scattering.

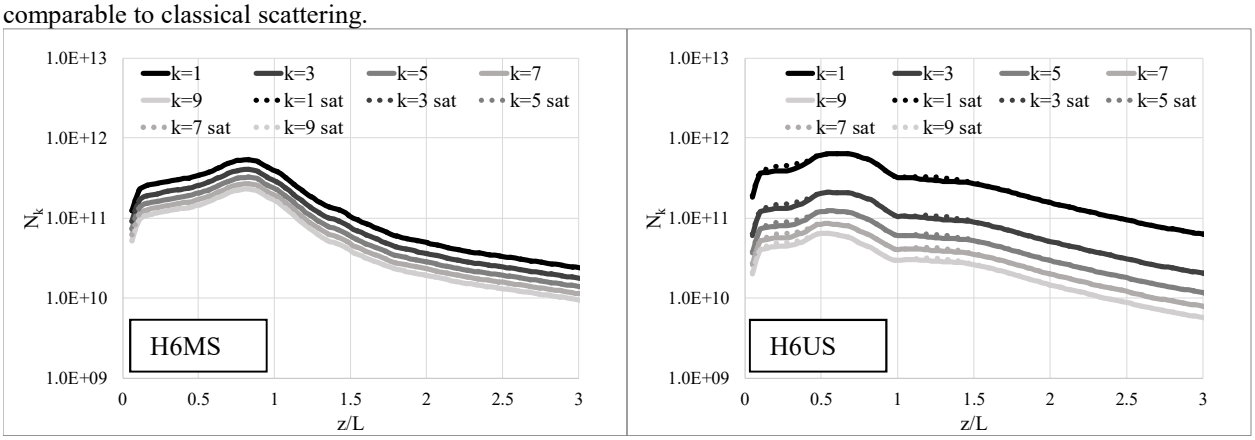

Figure 2. Comparison along channel centerline of the wave action at varying wavelengths for the H6MS and H6US at 300 V and 20 A. k=x corresponds to wavenumber x*500 m^{-1}

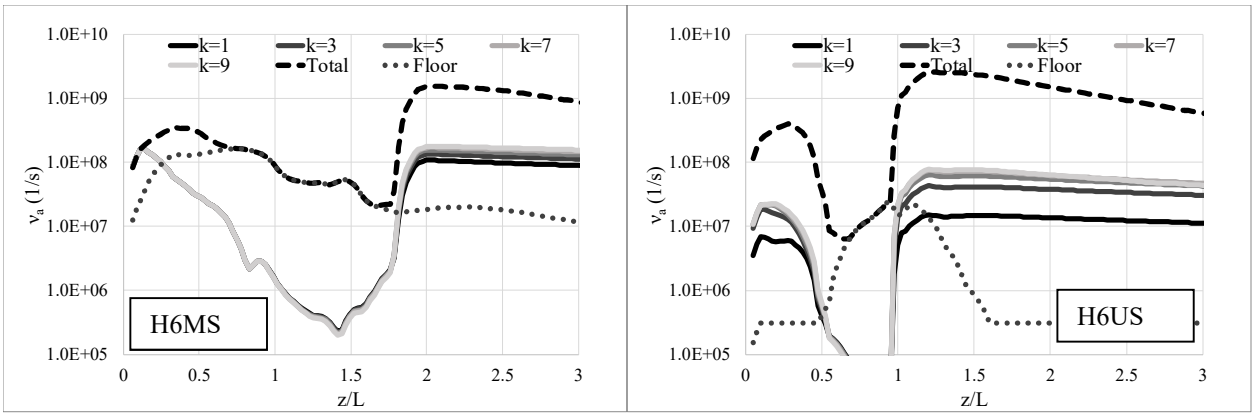

Figure 3. Comparison along channel centerline of the contribution to the anomalous collision frequencies of multiple wavelengths for the H6MS and H6US at 300 V and 20 A. Also included are the total anomalous collision frequency and the value of the floor anomalous collision frequency according to Eq. (15)

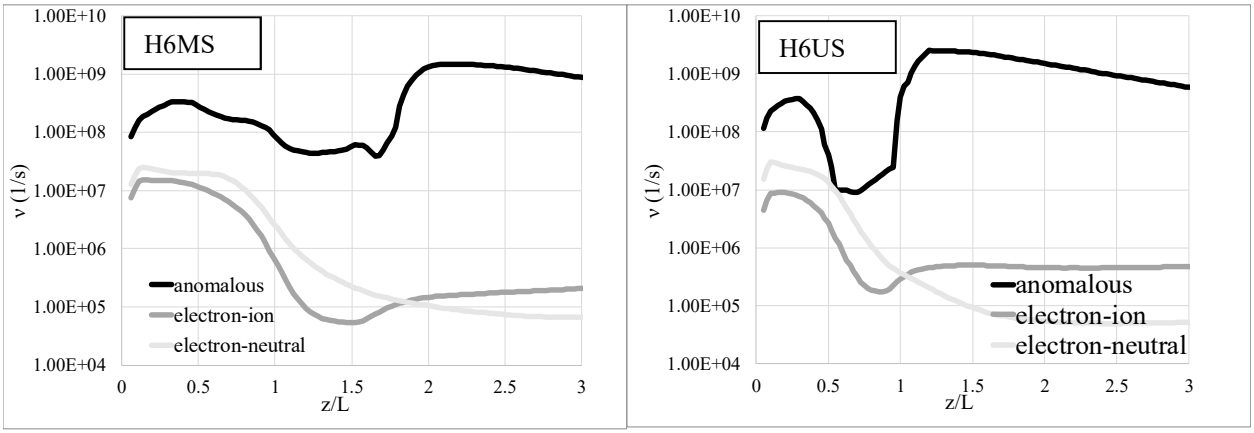

Figure 4. Anomalous collision frequency, ν_a at 300 V and 20 A and comparison with electron-ion, ν_{ei} and electron-neutral, ν_{en} collision frequencies. Left: H6MS, right: H6US

In Fig. 5, we present the computed results for plasma potential, electron temperature, and plasma density along the channel centerline for the H6MS and H6US operating at 300 V and 20 A. As expected by the anomalous collision frequency profiles of Fig. 4, the acceleration region is shifted in the H6MS. We notice that the increase in anomalous collision frequency as f moves from 0 to 1 controls the end of the steep gradient in plasma potential. The maximum electron temperature, which is driven by Joule heating, is recovered at the location of the steepest plasma potential. Finally, the plasma density also decreases across the acceleration region as predicted by mass conservation.

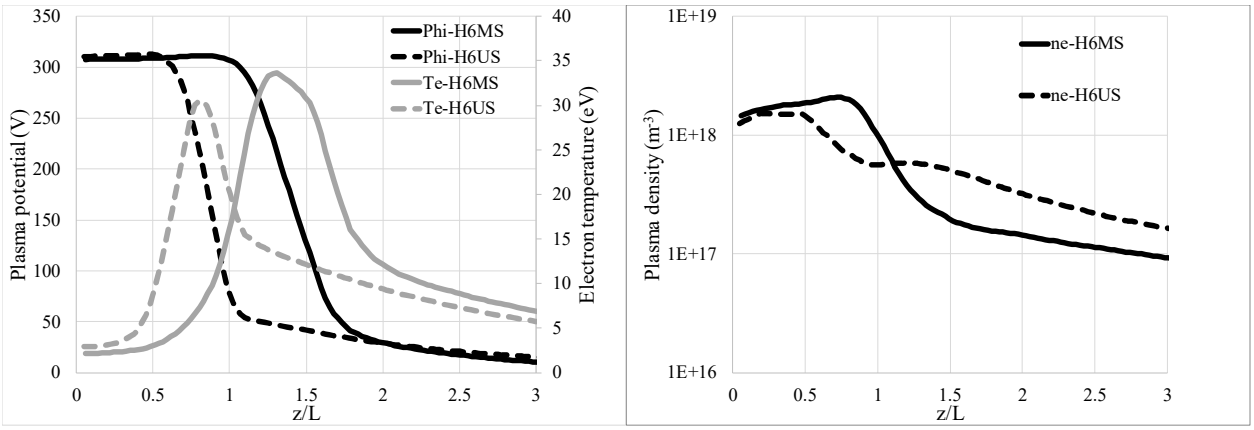

Figure 5. Comparison along channel centerline of the plasma potential, electron temperature, and plasma density for the H6MS and H6US at 300 V – 20 A.

Up to this point, we have shown that the first-principles model qualitatively behaves in the manner observed in experiments when the location of the peak magnetic field along the channel centerline changes. For additional confirmation of the accuracy of our numerical simulations, in Fig. 6 we depict a comparison between our simulation results and experimental measurements obtained with the use of LIF. Our model, when included in Hall2De, almost exactly matches the measured location of the acceleration region in the H6MS at 300 V and 20 A. For the H6US, LIF measurements were not available, but the location of the acceleration region was found to agree with the location inferred from wall probe measurements of the electron temperature to within 10% of the length of the acceleration channel.

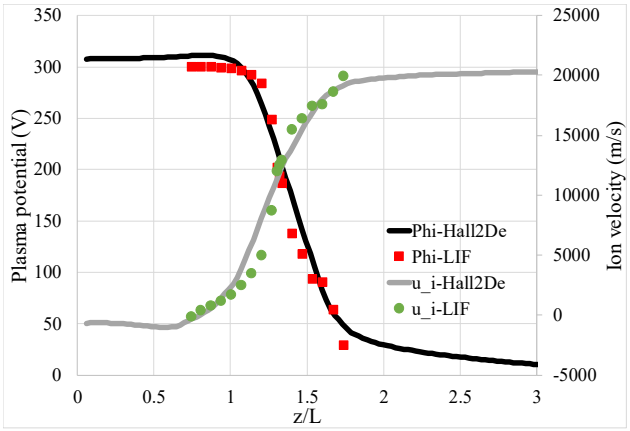

Figure 6. Comparison along channel centerline between Hall2De results for plasma potential and ion velocity and experimental results from LIF for the H6MS at 300 V and 20 A.

B. H6MS results at multiple operating conditions and comparison with experiments

In this subsection, we present the results of simulations run for the H6MS at multiple operating conditions and comparisons with the plasma potential profiles along the channel centerline derived from LIF measurements. In the LIF campaign, the thruster was operated at a constant current level of 15 A and increasing discharge voltage from 300 to 600 V. In addition, the thruster was also run at 800 V with lower current (11.25 A) as to not exceed the maximum power setting of 9 kW. Figure 7 depicts the results of these simulations in the form of the plasma potential profiles along the channel centerline. We show in the right panel the anomalous collision frequency, as computed by the first-principles model. The profiles obtained from LIF suggest that the plasma potential profiles below 300 V are very similar for all operating conditions. This feature was also observed in LIF measurements conducted for HERMeS [24]. The location of maximum acceleration, given by the steepest part of the plasma potential gradient, moves upstream with voltage (i.e., the steepest part of the profile for the 400 to 600-V operating conditions occurs for potential values above 300 V, near the upstream edge of the acceleration region). Thus, the acceleration region begins further upstream

with increased voltage but all the plasma potential profiles converge below 300 V. The Hall2De simulations do not capture this behavior, predicting instead an almost constant plasma potential gradient in the acceleration region. The difference between simulations and experiment in the acceleration region is more noticeable at higher discharge voltages because the change in curvature in the experimental plasma potential profile is larger. Nonetheless, the location of the acceleration region, defined as the region between flat plasma potentials, is accurately captured. To understand the reasons why we do not capture the accurate shape of the plasma potential in the acceleration region, we focus on how the anomalous collision frequency should look to capture the experimental profile. As shown in Fig. 7 (right), there exists an abrupt transition in the anomalous collision frequency at approximately z/L=1.7 for all the operating conditions. This abrupt change marks the transition from the region of high to low resistivity in the plasma. In order to draw electrons from the plume to the anode, the plasma potential increases accordingly in the high resistivity region. The value of the computed anomalous collision frequency is approximately constant from z/L =1 to z/L = 1.7, resulting in approximately constant resistivity and in turn a uniform gradient of the plasma potential (i.e., uniform electric field). In order to produce results more similar to the experiments, the transition from low to high resistivity at z/L=1.7 must be more gradual. In addition, the minimum anomalous collision frequency must be found close to the upstream boundary of the acceleration region, where the steepest gradients occur. In our model, the transition at z/L=1.7 transition occurs abruptly due to the exponential dependence built into the f function (Eq. (13)). We must note that Eq. (13) was written so we can capture the correct behavior in regions of f=1 and f=0. However, the transition between the two regions is completely dependent on the functions we chose to employ. We could have improved the agreement of our simulations by choosing a different functional for (13) but this exercise would have been purely phenomenological and would not have contributed to gaining insight on the physics that control the transition between the plume and the acceleration regions. Instead, it is our intention to use the PIC simulations described in our companion article [16] to improve our understanding of the acceleration region and produce an enhanced model for hydrodynamics codes building on the one presented in this article.

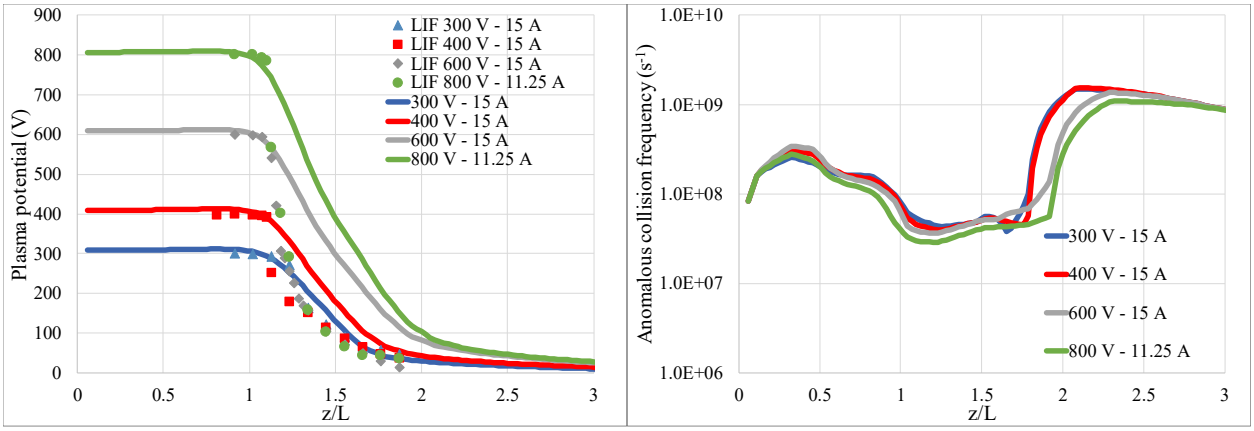

Figure 7. Left: Plasma potential along channel centerline and comparison with plasma potential obtained from LIF measurements of the ion velocity density distribution for the H6MS at multiple operating conditions. Right: Computed anomalous collision frequency for the H6MS at multiple operating conditions.

V. First-principles hydrodynamics simulations of HERMeS

The Hall Effect Rocket with Magnetic Shielding (HERMeS) [21] is part of an Ion Propulsion System (IPS) [22] currently under development through the Advanced Electric Propulsion System (AEPS) contract with Aerojet Rocketdyne. Work is being conducted at NASA Glenn Research Center (GRC) and Jet Propulsion Laboratory (JPL) to provide insight/oversight and testing support of the contract as well as risk reduction and life qualification activities. HERMeS is a 12.5 kW-class thruster that is operated at a nominal discharge current of 20.8 A and discharge voltage range from 300 to 600 V. The specifications for HERMeS also require stable operation at magnetic field strengths between 75% and 125% of the nominal value. In the first subsection, we conduct a study similar to that in Subsection IV b, in which we compare our numerical results with experimental measurements at constant current and magnetic

field with varying discharge voltage. In the second subsection, we investigate the behavior of the first-principles model when running simulations at constant discharge current and voltage with varying magnetic field strength.

A. Simulations at nominal magnetic field and varying discharge voltage

We show in Fig. 8 the comparison between numerical results and experimental measurements (from LIF measurements of the ion velocity distribution function [24, 26]) of the plasma potential profiles along the channel centerline for HERMeS at 300 V and 600 V, discharge current of 20.8 A and nominal magnetic field. We also include the computed anomalous collision frequency and a comparison of the plasma density and temperature for the two operating conditions. As we also found in the H6MS simulations, the location of the acceleration region is computed accurately. However, like in those simulations we do not capture the experimentally observed increasing gradient in the plasma potential in the direction of motion of the electrons. The features of the anomalous collision frequency and its relation to the plasma potential also bear similarities to the H6MS simulations. The boundary between acceleration region and plume is defined by a sharp transition between low and high resistivity (f=0 and f=1 in Eq. (13)). This sharp transition immediately increases the plasma potential gradient in our simulations. At 600 V, the differences between simulation and experiment are more acute due to the larger change in curvature that occurs at this condition compared to the 300-V condition. Similarly to the H6MS, the peak electron temperature is found at the same location as the steepest plasma potential. The maximum value of the temperature is higher at 600 V because Joule heating is proportional to the discharge voltage.

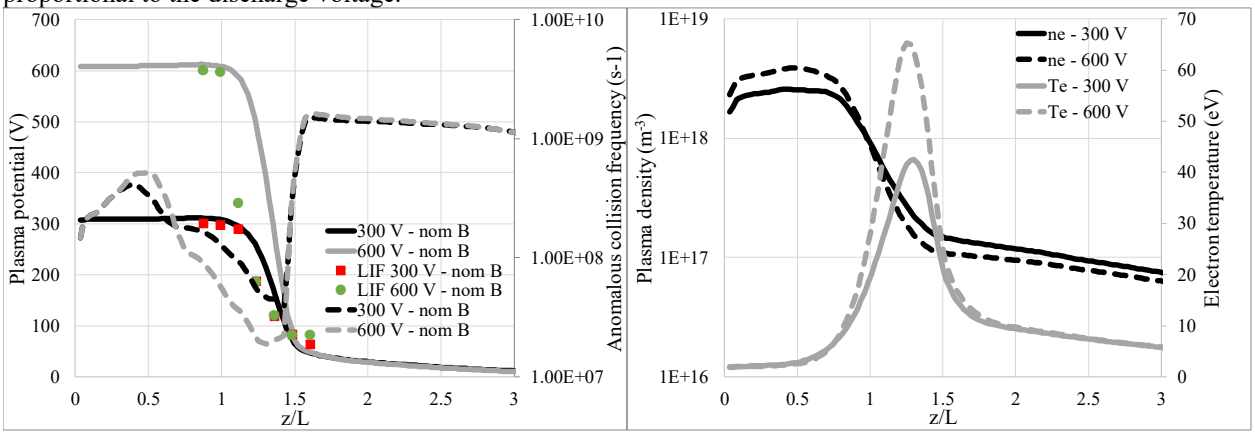

Figure 8. Left: Comparison along channel centerline of the computed plasma potential and anomalous collision frequency for HERMeS at 300 V – 20.8 A and nominal magnetic field. Plasma potential obtained from LIF measurements of the ion velocity distribution function are included. Right: Comparison along the channel centerline of the computed plasma density and electron temperature for HERMeS at 300 V – 20.8 A and nominal magnetic field.

B. Simulations at varying magnetic field

In this subsection, we compare the results of first-principles simulations at varying magnetic field for 300 V and 600 V with experimental measurements. The general trend observed in the experimental plasma potentials is that the acceleration region moves upstream with increasing magnetic field. The variation in location is albeit generally small, typically less than 5% of the channel length. However, we find that our numerical simulations cannot capture this trend, producing very similar plasma potential profiles in all cases (Fig. 9 for 300 V and Fig. 10 for 600 V). Examining the anomalous collision frequency profiles (right panels of Figs. 9 and 10), we notice small differences in the high resistivity region. As predicted by Eq. (15), when the magnetic field increases, so does the floor anomalous collision frequency. However, this small variation in the floor of the anomalous collision frequency does not appear to have a significant effect on the resistivity and consequently on the plasma potential. Since the physics that drive the variation in location of the acceleration region with magnetic field strength are not currently understood, it is hard to predict what improvements in the model may lead to a more accurate formulation that could capture the small shifts in location that have been experimentally observed. We are confident that the PIC code that we recently developed [16] can be a valuable tool for this purpose as it allows for variations in the profile and magnitude of the applied magnetic field.

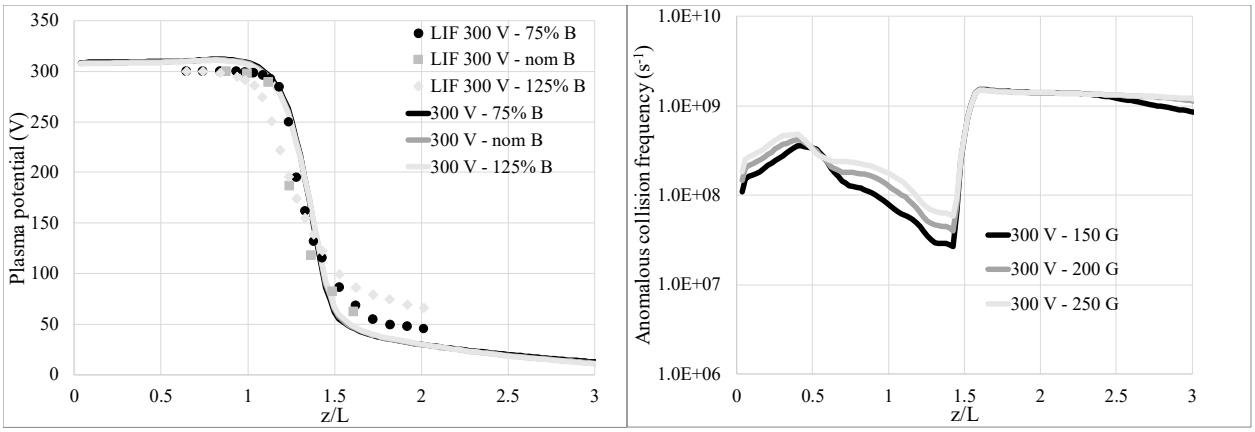

Figure 9. Left: Comparison along channel centerline of the plasma potential of Hall2De simulations of HERMeS at 300 V – 20.8 A and varying magnetic field. Plasma potential obtained from LIF measurements of the ion velocity distribution function are included. Right: Computed anomalous collision frequency along the channel centerline for HERMeS at 300 V – 20.8 A and varying magnetic field.

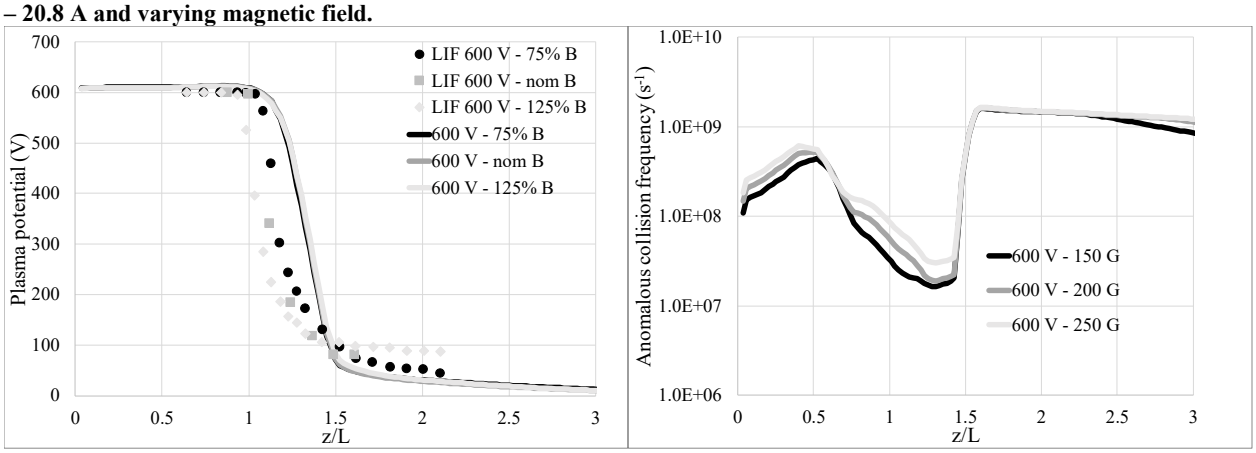

Figure 10. Left: Comparison along channel centerline of the plasma potential of Hall2De simulations of HERMeS at 600 V – 20.8 A and varying magnetic field. Plasma potential obtained from LIF measurements of the ion velocity distribution function are included. Right: Computed anomalous collision frequency along the channel centerline for HERMeS at 600 V – 20.8 A and varying magnetic field.

VI. Conclusions

In [17], we presented a physics-based model based on a pseudo-particle description of ECDI. Numerical simulations using Hall2De showed promising results for the unshielded H6 thruster. In this article, we extended our investigations to two different thrusters and multiple operating conditions with the aim of confirming that the results obtained for the H6 could be replicated more generally. A key improvement of the model with respect to previous work is that linear theory is not applied in the event of wave saturation and deviations of electrons or ions from a Maxwellian distribution function. In the acceleration region, the anomalous collision frequency is computed as the minimum value necessary to prevent the electron drift velocity from exceeding the thermal velocity and a functional based on the electron equilibration time is defined to control the transition from the high to the low resistivity regions (i.e., from the acceleration to the plume regions).

The first thruster investigated was the H6MS, a magnetically shielded version of the H6US used in [16]. Our simulations showed that the model was capable of capturing accurately the location of the acceleration region for the nominal operating condition of 300 V and 20 A. When the model was applied to higher discharge voltages, we found that even though the location of the acceleration region was still captured, fine details, such as the progressive increase in the steepness of the plasma potential gradient in the direction of motion of the electrons, were not replicated in our simulations. We determined by examination of the computed anomalous collision frequency profile that a smoother transition between the low and the high resistivity regions would lead to numerical solutions closer to the experimental measurements.

The investigations with the HERMeS thruster geometry and comparisons with LIF allowed us to explore the behavior of our model with varying magnetic field strength (at fixed location of the peak magnetic field along the channel centerline). Here, experiments show small shifts in the location of the acceleration region (less than 5% of the length of the acceleration channel) at varying magnetic field (for a range than spans 75% to 125% of the nominal magnetic field value). This effect was not captured in our simulations, which exhibited minimal sensitivity to changes in the magnetic field.

We consider fulfilled our main goal of verifying that the model presented in [17] was general enough that the location of the acceleration region is accurately captured in simulations of a variety of Hall thrusters and operating conditions. We have also identified two weaknesses of our model that were not apparent in [17]. First, the model did not capture the experimentally observed progressive increase in steepness of the acceleration region in the direction of motion of the electrons (i.e., from the plume to the anode), a phenomenon better observed at large discharge currents. Second, the model lacks the observed sensitivity to varying magnetic field strengths. We envision that the 2-D PIC model of the acceleration and plume regions presented in [16] will be used as a tool to gain insight on the physics that drive these phenomena and that these investigations will lead to a more accurate first-principles model in the near future.

Acknowledgments

The authors would like to thank Dr. Wensheng Huang and Dr. Benjamin Jorns for producing some of the experimental measurements that were employed in this manuscript. The research described in this paper was carried out by the Jet Propulsion Laboratory, California Institute of Technology, under a contract with the National Aeronautics and Space Administration. The support of the joint NASA GRC and JPL development of the Advanced Electric Propulsion System by NASA's Space Technology Mission Directorate through the Solar Electric Propulsion Technology Demonstration Mission project is gratefully acknowledged.

References

[1] Mikellides, I. G. and Katz, I., "Numerical Simulations of Hall-effect Plasma Accelerators on a Magnetic-Field-Aligned Mesh", Physical Review E, Vol. 86, 2012, p. 046703, doi: 10.1103/PhysRevE.86.046703

[2] Lopez Ortega, A. and Mikellides, I. G., "The Importance of the Cathode Plume and its Interactions with the Ion Beam in Numerical Simulations of Hall Thrusters", *Physics of Plasmas*, Vol. 23, 043515, 2016, doi: 10.1063/1.4947554

[3] Heron, A., and Adam, J. C., "Anomalous Conductivity in Hall Thrusters: Effects of the Non-linear Coupling of the Electron-Cyclotron Drift Instability with Secondary Electron Emission of the Walls", Physics of Plasmas, Vol. 20, 082313, 2013, doi: 10.1063/1.4818796

[4] Adam, J. C., Heron, A., and Laval, G., "Study of Stationary Plasma Thrusters Using Two-dimensional Fully Kinetic Simulations", Physics of Plasmas, Vol. 11, 2004, 295, doi: 10.1063/1.1632904

[5] Coche, P. and Garrigues, L., "A Two-Dimensional (Azimuthal-Axial) Particle-In-Cell Model of a Hall Thruster", Phys Plamas 21, 023503, 2014, doi: 10.1063/1.4864625

[6] Forslund, D. W., Morse, R. L., and Nielson, C. W., "Electron Cyclotron Drift Instability," *Physical Review Letters,* Vol. 25, no. 18, pp. 1266, 1970, doi: 10.1103/PhysRevLett.25.1266

[7] Bychenkov, V. Y., Silin, V. P., and Uryupin, S. A., "Ion-acoustic Turbulence and Anomalous Transport", *Physics Reports*, Vol. 164, Issue 3, 1988, 199-215, doi: 10.1016/0370-1573(90)90122-I

[8] de Kluvier, H., Perepelkin, N. F., and Hirose, A., "Experimental Results on Current-driven Turbulent Plasmas – a Survey", *Physics Reports*, Vol. 199, Issue 6, 1991, 281-381, doi: 10.1016/0370-1573(91)90060-Y

[9] Stix, T. H., *Waves in Plasmas*, Springer-Verlag, New York, 1992.

[10] Horton, H., *Turbulent transport in magnetized plasmas*, World Scientific, Singapore, 2012.

[11] Tsikata, S., Lemoine, N., Pisarev, V., and Gresillon, D. M., "Dispersion Relation of Electron Density Fluctuations in a Hall Thruster Plasma, Observed by Collective Light Scattering", *Physics of Plasmas*, Vol. 16(3), 033506, 2009, doi: 10.1063/1.3093261

[12] Cavalier, J., Lemoine, N., Bonhomme, G., Tsikata, S., Honore, C., and Gresillon, D., "Hall Thruster Plasma Fluctuations Identified as the ExB Electron Drift Instability: Modeling and Fitting on Experimental data", *Physics of Plasmas*, Vol. 20, 082107, 2013, doi: 10.1063/1.4817743.

[13] Ducrocq, A., Adam, J. C., Heron, A., and Laval, G., "High-Frequency Electron Drift Instability in the Cross-Field Configuration of Hall Thrusters", *Physics of Plasmas*, Vol. 13(10), 102111, 2006, doi: 10.1063/1.2359718.

[14] Lafleur, T., Baalrud, S. D., and Chabert, P.," Theory for the Anomalous Electron Transport in Hall Effect Thrusters. I. Insights from Particle-In-Cell Simulations", *Physics of Plasmas*, Vol. 23, 053502, 2016, doi: 10.1063/1.4948495

[15] Lampe, M., Manheimer, W. M., McBride, J. B., Orens, J. H., Papadopoulos, K., Shanny, R., and Sudan, R. N., "Theory and Simulation of the Beam Cyclotron Instability", Physics of Fluids, Vol. 15, No. 4, 1972, doi: 10.1063/1.4972269.

[16] Katz, I., Chaplin, V. H., and Lopez Ortega, A., "Numerical Studies of Hall Thruster Acceleration Region Electron Transport", AIAA 2018-xxxx, July 2018

[17] Lopez Ortega, A., Katz. I, and Chaplin, V. H, "A First-Principles Model Based on Saturation of the Electron Cyclotron Drift Instability for Electron Transport in Hydrodynamics Simulations of Hall Thruster Plasmas", IEPC paper 2017-178, October 2017.
[18] Haas, J. M., Hofer, R. R., Brown, D. L., B, Reid, B. M., and Gallimore, A. D., "Design of a 6-kW Hall thruster for high thrust/power investigation", in 54th JANNAF Propulsion Meeting, Denver, Colorado, 2007.
[19] Mikellides, I.G., Katz, I, and Hofer, R.R, "Design of a laboratory Hall thruster with magnetically shielded channel walls, phase I: numerical simulations", AIAA paper 2011-5809, July 2011.
[20] Hofer, R. R., Goebel, D. M., Mikellides, I. G., and Katz, I., "Design of a Laboratory Hall Thruster with Magnetically Shielded Channel Walls, Phase II: Experiments", AIAA paper 2012-3788, July 2012.
[21] Hofer, R. R., Polk, J. E., Sekerak, M. J., Mikellides, I. G., Kamhawi, H., Sever-Verhey, T. R., Herman, D. A., and Williams, G., "The 12.5 kW Hall Effect Rocket with Magnetic Shielding (HERMeS) for the Asteroid Redirect Robotic Mission", AIAA paper 2016-4825, July 2016.
[22] Herman, D., Tofil, T., Santiago, W., Kamhawi, H., Mcguire, M., Polk, J. E., Snyder, J. S., Hofer, R., Picha, F., Jackson, J., and Allen, M., "Overview of the Development and Mission Application of the Advanced Electric Propulsion System (AEPS)," IEPC-2017-284, October 2017.
[23] Jorns, B. A., Dodson, C. A., Anderson, R. A., Goebel, D. M., Hofer, R. R., Sekerak, J. M., Lopez Ortega, A. and Mikellides, I. G., " Mechanisms for Pole Piece Erosion in a 6-kW Magnetically Shielded Hall Thruster", AIAA paper 2016-4839, July 2016.
[24] Chaplin, V. H, Jorns, B. A., Conversano, R. W., Lobbia, R. B., and Lopez Ortega, A., "Laser Induced Fluorescence Measurements of the Acceleration Zone in the 12.5 kW HERMeS Hall Thruster", IEPC 2017-229, October 2017.
[25] Mikellides, I. G. , Katz, I., Hofer, R. R., Goebel, D. M., de Grys, K. H., and Mathers, A., "Magnetic Shielding of the Channel Walls in a Hall Plasma Accelerator," Physics of Plasmas, Vol. 18, no. 3, pp. 033501, 2011, doi: 10.1063/1.3551583
[26] Huang, W., Kanhawi, H., and Herman, D. A., "Ion Velocity Distribution in the Channel and Near-Field of the HERMeS Hall Thruster", AIAA paper 2018-xxxx, July 2018